JOURNAL OF MATERIALS SCIENCE **36** (2001) 5315–5323

Microstructural evolution in rapidly solidified Al-Cu-Si ternary alloys

K. P. COOPER, H. N. JONES, III
Materials Science and Technology Division, Code 6324, Naval Research Laboratory, 4555 Overlook Avenue, SW, Washington, DC 20375-5343, USA
E-mail: cooper@anvil.nrl.navy.mil

Several Al-Cu-Si alloys were melt spun to produce stable, fine scale microstructures suitable for superplastic deformation and consolidation. Scanning electron microscopy of the ribbon cross-sections reveal two distinct alternating microstructural morphologies, suggesting transitions in solidification behavior. One structure consists of intimately interlocked α-Al and θ (Al_2Cu) phases with dispersed spheroids of (Si). The other structure consists of equiaxed or cellular-dendritic α-Al with interdendritic θ and (Si). The latter was found in the middle portion of the ribbon cross-section when cast at a low speed, and throughout the ribbon cross-section when cast at high speed. The dendritic structure appears to result from independent nucleation events in the undercooled liquid ahead of the solid-liquid interface. The solidification mechanism for the interlocked structure appears to involve multiple nucleation of the θ phase followed by its cooperative growth with the α-Al phase. This cooperative growth is unlike that which forms a lamellar structure, as it results in a branched, randomly oriented network. We postulate that the (Si) phase is the first phase to form from the undercooled liquid, and it is uniformly dispersed throughout the undercooled melt. The (Si) spheroids provide nucleation sites for the θ phase because of its observed association with the θ phase. The α-Al grain size varies from 1 μm near the wheel side surface of the ribbon to 8 μm with sub-grains near the free surface. The size of the θ and (Si) phases is on the order of a μm and less. The microstructural size scale appears to be small enough for this material to exhibit superplastic behavior when deformed.

1. Introduction

Superplastic deformation of metals is useful in forming near net shapes with consequent cost savings because of the ease of forming and reduced amount of post-deformation processing required. Several aluminum alloys have been commercially exploited for superplastic forming as several binary and ternary eutectic alloys have been shown to exhibit superplasticity. A review of superplastic aluminum alloys was given by Wadsworth *et al*. [1]. The superplastic behavior of Al-Cu binary alloys has been studied extensively, particularly the Al-32 wt% Cu eutectic alloy. This and other eutectic alloys became model systems because of the emphasis on approximately equal volume fractions of the two phases to avoid rapid grain growth, and because of the relative ease with which the lamellar structure could be thermomechanically processed into fine-grained, two-phase mixtures.

The constitutive relationship for superplastic flow and slip creep [2] is given by,

$$\dot{\varepsilon} = Ad^{-p}D\left(\frac{\sigma}{E}\right)^{n}, \qquad (1)$$

where $\dot{\varepsilon}$ is the optimum strain rate, A is a material constant, d is the grain size, p is the grain-size dependence (typically 2-3), D is the diffusivity, σ is the stress, and E is the elastic modulus. According to this relationship, refinement in grain size by a factor of two is expected to increase the optimum strain rate for superplastic flow by a factor of four to eight. Nieh and Wadsworth [3] demonstrated that by reducing the grain size in aluminum alloys, optimal superplastic flow was possible at high strain rates. Because a fine-grained morphology is a requirement for superplastic behavior, rapid solidification processing was introduced to produce materials with very fine grain structure. It was found that rapid solidification did not always result in superplasticity because the refined microstructure does not always include high angle grain boundaries needed for grain boundary sliding, a predominant mode of deformation for superplastic flow according to Wadsworth and Pelton [4]. However, an advantage of rapid solidification is the ability to produce particulate material with an extremely fine-grained, stable microstructure, and hot press or extrude the aggregate at a suitable temperature and strain rate into the final shape in a single step. Superplastic flow during consolidation would result in a fully dense, high strength, high performance component. Unlike the ingot metallurgy route which involves several processing steps when fabricating parts—casting, hot

working, rough machining, heat treatment and final machining, superplastic consolidation required fewer steps yielding components at reduced cost.

The most common technique for making very fine-grained material is by freezing the melt at a rapid rate. The melt spinning process is an effective method for achieving rapid quench rates and it produces microstructures very different from those formed in slow-cooled bulk material. Depending upon the alloy composition and the ribbon thickness, cooling rates range between 10^5 to 10^8 K/sec for this technique [5]. When cooling rates approach these values, non-equilibrium, metastable and amorphous microstructures are possible [6]. Supersaturated solid solutions, fine-scale phase distributions and ultra-fine grain size have also been reported [7]. In this work, melt spinning was used primarily to form fine-scale phase dimensions and distributions.

2. Selection of alloy system

Studies of Al-Cu alloys have investigated fundamentals of the eutectic reaction [8], rapid solidification [9] and superplastic behavior [10]. The Al-Cu-Si ternary system is a natural extension of the Al-Cu binary system that introduces several improvements. The equilibrium phases in the ternary Al-Cu-Si alloy system are α-Al, θ phase (Al_2Cu) and (Si) phase. There is no ternary compound that could lead to embrittlement. The solubilities of Cu in the (Si) phase and of Si in the θ phase are negligible, which is desirable as this limits coarsening of these phases during thermomechanical processing. The presence of Si improves fluidity, making it easier to cast these alloys. According to Mondolfo [11], Si also increases the number of dislocation loops in Al-Cu alloys and tends to accelerate the age hardening process, thus increasing the strength.

A portion of the Al-Cu-Si ternary diagram, taken from Mondolfo [11] is given in Fig. 1. It shows the liquidus lines, isotherms and alloys investigated. In addition to the binary Al-Cu and the ternary Al-Cu-Si eutectic compositions, alloys along the Al-Si liquidus were studied. Experimental run designations, alloy compositions and estimated fractions of the phases are given in Table I. Alloy compositions were selected with the following criteria in mind:

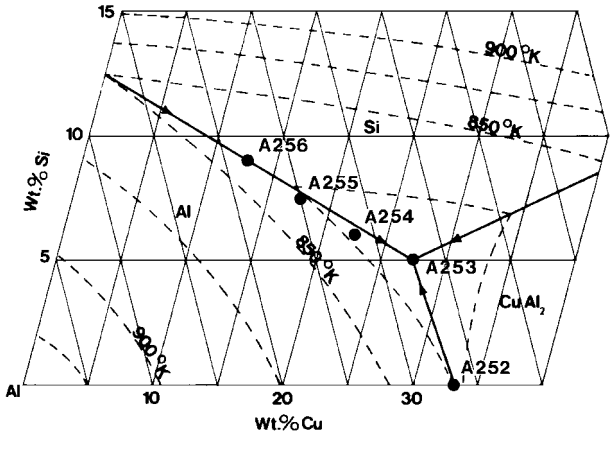

Figure 1 The aluminum corner of the Al-Cu-Si phase diagram showing the liquidus troughs, temperature isotherms and phase fields[11]. The closed circles correspond to the experimental alloys.

TABLE I Run designations, alloy compositions and phase fractions for experiments

	Composition (wt%)			Estimated phase fractions (vol%)			
Alloy designation	Al	Cu	Si	α-Al	θ	(Si)	θ + (Si)
A252 Al-Cu binary eut.	68	32	–	41	59	–	59
A253 Al-Cu-Si ternary eut.	67.5	27.5	5	44	51	5	56
A254	71.5	22.5	6	52	42	6	48
A255	75	17.5	7.5	60	32	8	40
A256	78.5	12.5	9	67	24	9	33

1) The optimum hard-phase volume fraction for very high strength materials that remain tough and ductile, should be in the vicinity of 30%. The hard-phase should be uniformly distributed and of very fine-scale. Hard-phase volume fraction greater than 40% results in a brittle material.

2) In Al-Cu, the eutectic alloy has a hard phase volume fraction of 59%, which is too high. In Al-Si, the eutectic alloy has a hard-phase volume fraction of 12%, which is too low.

3) Compositions near the ternary eutectic were chosen to promote coupled growth, which is necessary for producing fine-grained microstructures.

3. Experimental procedure

The binary and ternary aluminum alloys listed in Table I were prepared by electric arc button melting under argon. The impurity content of the alloys was held very low by using 99.99% pure starting materials. The buttons were sliced, and slices totaling 20 g were placed in a graphite crucible, induction melted, and ejected through a 0.75 mm diameter orifice in the crucible onto a Cu-Be alloy spinning wheel. The wheel had a 600 grit surface finish to allow for good thermal contact between the melt and the wheel surface. The surface velocity of the spinning wheel was 15 m s^{-1} for most experiments. For Alloy A255, speeds of 6, 15 and 50 m s^{-1} were used to investigate the effect of wheel speed on microstructure formation. Melt spinning was done in a partial He gas environment so there was little oxidation of the ribbon. For microstructural analysis, the ribbon samples were mounted in stainless steel clamps and cross-sections were ground and polished, with the final polish being with 0.5 μm diamond paste. The as-polished samples were examined in a high resolution scanning electron microscope (SEM). Back-scattered imaging was used to reveal the phase distributions. Foils of some of the ribbon samples were prepared by ion milling and examined in the transmission electron microscope (TEM). Microstructural evaluation involved identification of the phases present and determination of their size, shape and spacing.

4. Results

The melt spun ribbons had very good edge definition. However, the edges were curled and in some cases thicker than the central portion of the ribbon. Ribbon dimensions varied with wheel speed, as shown in Table II.

TABLE II Melt spun ribbon dimensions

Wheel speed (m s^{-1})	Ribbon thickness (μm)	Ribbon width (mm)
6	60	6
15	25–40	4.5
50	25	3

The ribbon thickness was found to be alloy-dependent, yielding the range of thicknesses at 15 m s^{-1} speed. For consistency, only the microstructure in the central portion of the ribbon was evaluated.

A variety of microstructures were observed in the melt spun ribbons. Typical ones are shown in Figs 2 and 3. These are SEM back-scattered images in which the dark phase is the α-Al phase and the light phase is the θ-Al_2Cu. Fig. 2a and b show the lamellar eutectic structure obtained in Alloy A252, which is the binary Al-Cu eutectic. The entire ribbon exhibited the lamellar structure. Fig. 2a shows the lamellar structure on the free surface of the ribbon where the eutectic colony grains are about 1 to 2 μm in diameter and the lamellar spacing is about 0.075 to 0.1 μm. These dimensions suggest that the local solidification rate was rapid in these samples. The lamellar morphology is revealed in cross-section, as shown in Fig. 2b. The growth direction in this image is upwards. By comparison, the microstructure in Alloy A253, which has the ternary Al-Cu-Si eutectic composition, appears as a fine mixture. Fig. 2c, which has the same magnification as Fig. 2b, shows the structure in cross-section. The microstructure is not lamellar and appears to be an irregular mixture of α-Al and θ phases, with a spacing of about 0.15 μm.

Microstructures formed in Alloy A255 melt spun ribbons cast at different wheel speeds are shown in Fig. 3. These are ribbon cross-sections, with the growth direction upwards. The images were taken at different magnifications so that the entire cross-section could be viewed, illustrating microstructural variations between the wheel-side (bottom) and the free surface (top) of the ribbon. The microstructure was found to

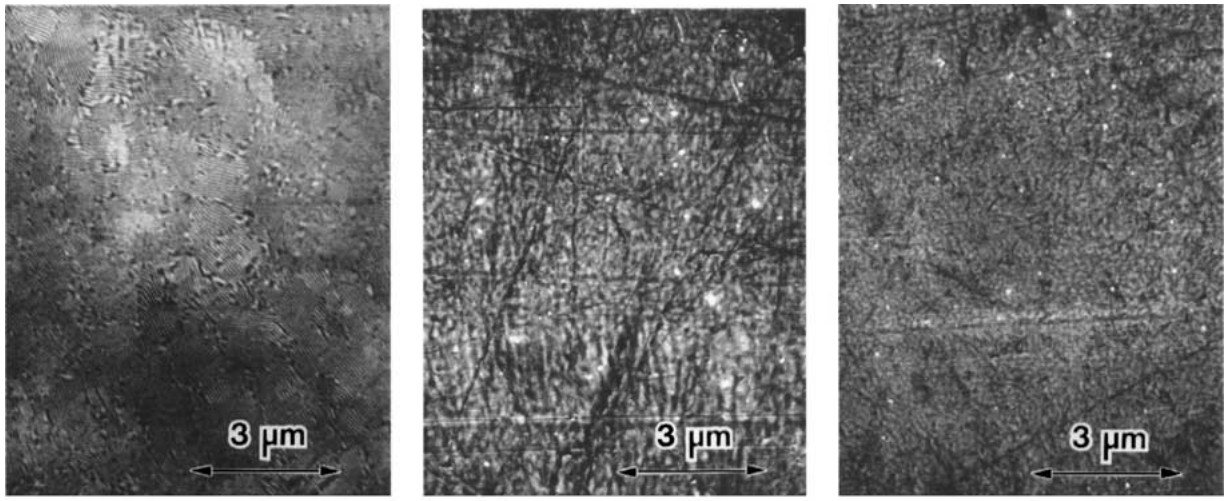

Figure 2 Eutectic microstructures in melt spun ribbon samples cast at 15 m s^{-1}. (a) and (b) Free surface and cross-section, respectively, of lamellar morphology in Alloy A252 having the binary Al-Cu eutectic composition on. (c) Irregular morphology in Alloy A253 having ternary Al-Cu-Si eutectic composition.

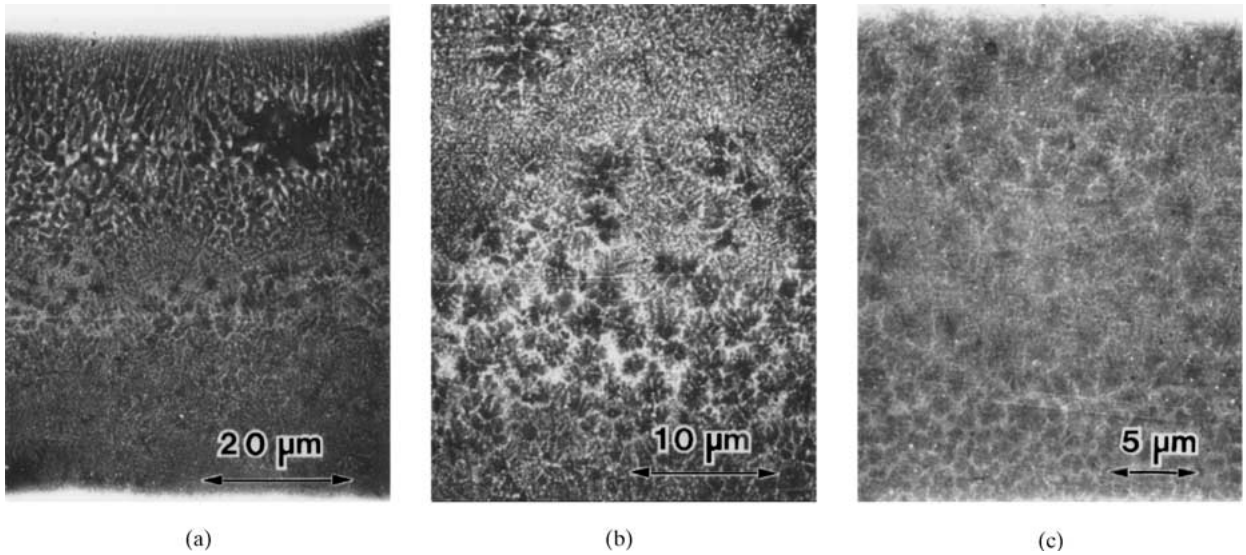

Figure 3 Microstructures obtained in Alloy A255 melt spun ribbons as a function of wheel speed. (a) 6 m s^{-1}. (b) 15 m s^{-1}. (c) 50 m s^{-1}.

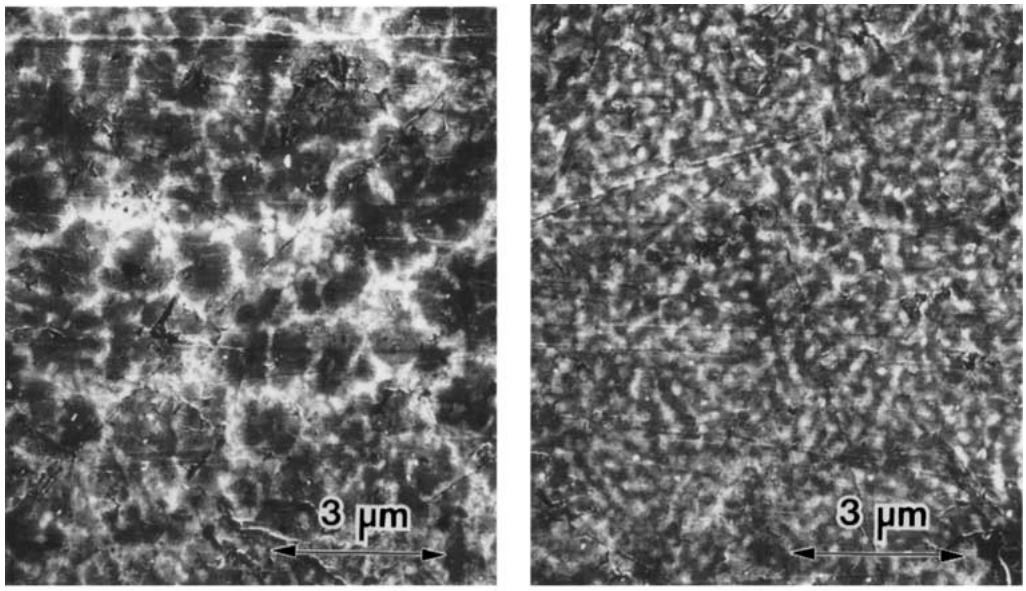

Figure 4 Morphologies observed in Alloy A255 melt spun with a speed of 15 m s^{-1}. (a) Cellular-dendritic. (b) Interlocked eutectic.

vary significantly as a function of wheel speed. Furthermore, the microstructure is not uniform within the ribbon cross-section. Two distinct morphologies were identified and their relative amounts varied with wheel speed. The two morphologies are shown in the high magnification micrographs of Fig. 4. Fig. 4a shows a morphology that we have termed "cellular-dendritic". It consists of dark, star-shaped α-Al dendrites with the lighter θ phase as the interdendritic material. Fig. 4b shows a morphology that we have termed "interlocked eutectic." It consists of an irregular arrangement of a two-phase eutectic mixture of the darker α-Al and the lighter θ phase. The scale and morphological distribution of this microstructure varied with wheel speed. These effects are not apparent from the micrographs in Fig. 3 because the magnifications are different for each micrograph. However, quantitative analysis of the microstructures demonstrated the variations in scale and phase distributions with wheel speed, and these results are shown in Fig. 5. The decrease in the eutectic spacing and in the eutectic volume fraction with wheel speed are shown in Fig. 5a and b, respectively. There is a decrease in the eutectic spacing with increasing copper content of the alloys, as shown in Fig. 6a. The eutectic volume fraction, however, appears to increase with increasing copper content as shown in Fig. 6b.

The alloy A255 sample, which was melt-spun at with an intermediate speed of 15 m s^{-1}, was further examined using the TEM. Fig. 7 shows TEM images of the structure near the free surface of the ribbon. Fig. 7a is a bright-field image showing the interlocked eutectic morphology. Fig. 7b is the dark-field version of Fig. 7a that reveals the α-Al grain and sub-grains. Fig. 7c is a high-magnification, dark-field image of the θ phase highlighting its unique morphology. Multiple branching of the θ phase is evident. Fig. 7d is a dark-field image of the (Si) phase, highlighting its size and distribution. The (Si) phase appears to be mostly associated with the θ phase. Near the wheel-side surface of the ribbon the θ phase appears as discrete particles, as shown in the bright-field image of Fig. 8. Fig. 9 shows dark field TEM micrographs highlighting the scale and shape of the α-Al grains in other regions of the melt spun ribbon. Fig. 9a is taken from the middle portion of the

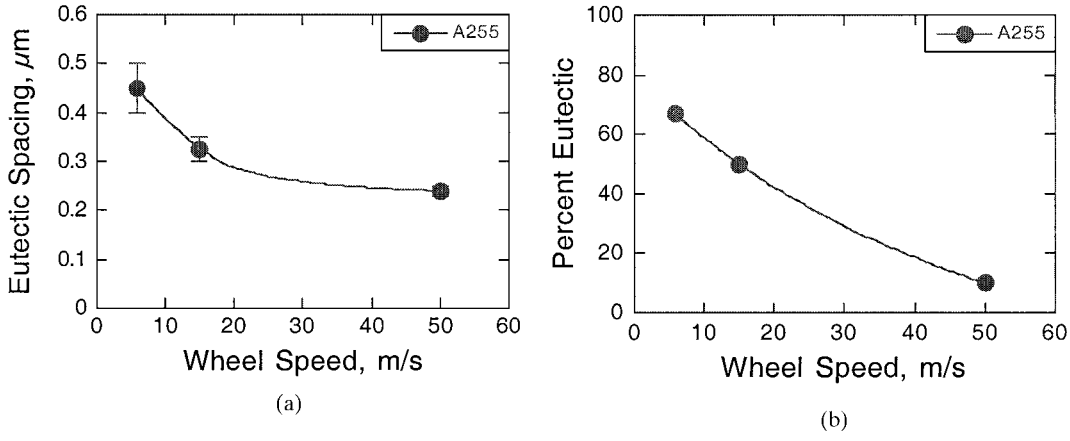

Figure 5 Variation in the scale and morphological distribution of the microstructure in Alloy A255 melt spun ribbons as a function of wheel speed. (a) Eutectic spacing. (b) Eutectic volume fraction.

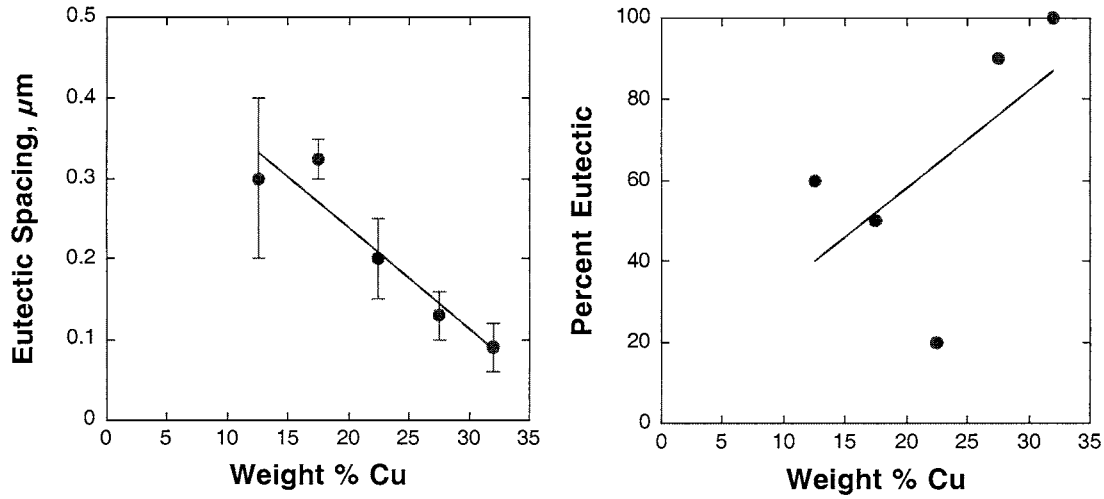

Figure 6 Scale and morphological distribution of the microstructure in the various alloys as a function of the copper content. (a) Eutectic spacing. (b) Eutectic volume fraction.

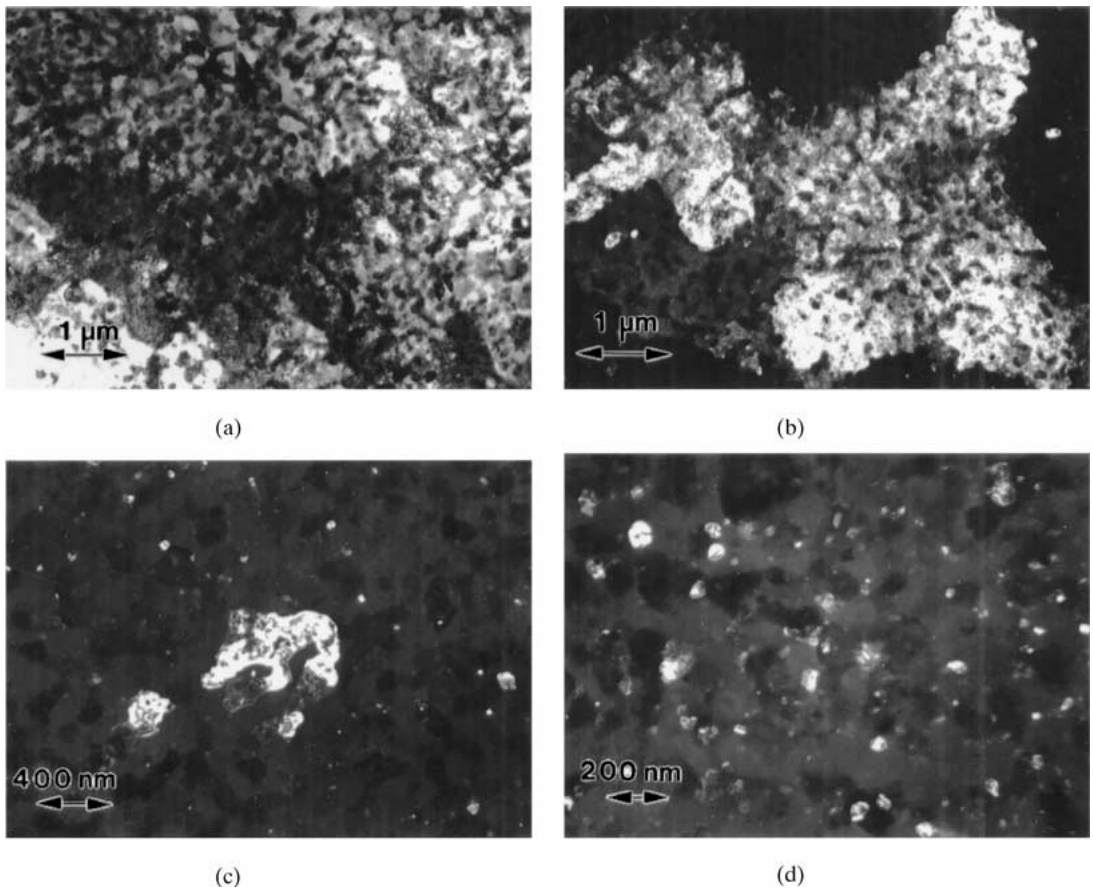

Figure 7 TEM micrographs near the top surface of Alloy 255 ribbon melt spun at 15 m s^{-1} showing the scale and morphology of the various phases present. (a) Bright field image showing the interlocked eutectic phase. (b) Dark field image showing the scale and shape of an α-Al grain. (c) Dark field image showing the size and shape of the θ phase. (d) Dark field image showing the size and distribution of the (Si) phase.

ribbon and, Fig. 9b from the wheel-side surface of the ribbon. A semi-quantitative analysis of the TEM microstructures is summarized in Table III. In general, the α-Al grains are equiaxed and sometimes they contain sub-grains. The α-Al grains increase in size from the wheel-side to the free surface of the ribbon. The morphology of the θ phase is elongated and cylindrical and, in some cases, branched. A greater degree of θ-phase branching is observed in the microstructure closer to the free surface of the ribbon. The size or thickness of the θ phase varies from 0.1 μm to 1.5 μm. The (Si) phase is mostly spherical with a diameter ranging from 0.05 μm to 1.2 μm. Unlike the α-Al grains, no general trend is observed in the size of the θ phase and the (Si) phase from wheel-side to the free surface.

We examined the interlocked eutectic structure in detail in the SEM using the back-scattered diffraction mode. The compositional differences of the three phases are easily highlighted, as shown in Fig. 10. The gray α-Al phase and the light θ phase appear

TABLE III Semi-quantitative analysis of the TEM micrographs

	α-Al grains		θ phase		(Si) phase	
Location in ribbon	Morphology	Size (μm)	Morphology	Size (μm)	Morphology	Size (μm)
Free surface	Equiaxed, subgrains	4.0–8.0	Cylindrical branched	0.5–0.7	Spherical	0.02–0.08
Middle	Equiaxed, no subgrains	2.0–4.0	Elongated	0.8–1.5	Spherical	0.7–1.2
Wheelside	Equiaxed, no subgrains	1.0–1.5	Elongated, cylindrical	0.1–0.2	Spherical	0.05–0.12

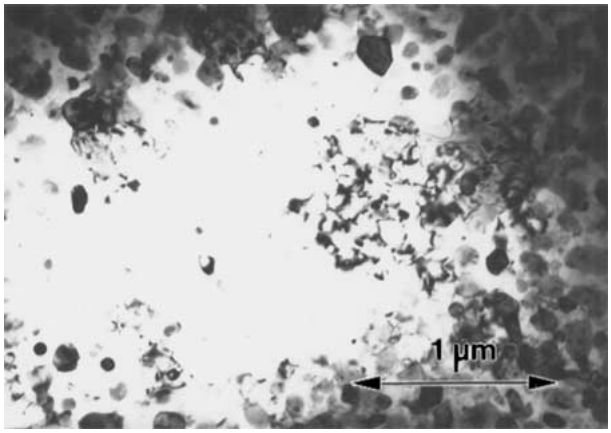

Figure 8 TEM bright field image of Alloy 255 ribbon melt spun at 15 m s^{-1} showing the scale, shape and distribution of the θ phase near the wheel-side surface.

in an intimately interlocked configuration. The small, dark spheroids of (Si) are scattered throughout the microstructure and appear mostly in or attached to the θ-phase, but never within the α-Al phase.

5. Discussion

The formation of a lamellar structure in the melt-spun binary Al-Cu eutectic alloy is not surprising. At the intermediate melt spinning speed, it appears that the undercooled melt was within the coupled growth region of the Al-Cu binary phase diagram prior to nucleation. Because the heat extraction is essentially one-dimensional through the copper wheel, the lamellar structure was aligned from the wheel-side to the free surface of the ribbon. However, in the ternary eutectic alloy, the lamellar structure was not observed. Instead, a fine-scale, irregular arrangement of the three phases was obtained throughout the ribbon cross-section. The presence of the third phase (Si) appears to inhibit lamellar growth. The irregular eutectic structure is similar to the interlocked structure observed in the off-eutectic composition alloys which are described in detail later.

The presence of two distinct morphologies, cellular-dendritic and interlocked eutectic, in the microstructure was typical of the off-eutectic composition alloy melt spun ribbons. A close examination of the micrographs in Fig. 3 reveals that these two morphologies occur as alternating bands. The "banded" structure and volume fraction variation with melt spinning speed suggest a complex solidification behavior. At the low wheel speed, the initial solidification structure is interlocked eutectic followed by alternating dendritic and eutectic bands. Fluctuations in undercooling levels ahead of the solidification front due to recalescence could lead to the banded structure. At higher wheel speeds, the initial solidification morphology is cellular-dendritic, with randomly oriented dendrites. There is no alignment of the dendrites in the heat flow direction which would signify a growth-dominated structure. These observations suggest that the cellular-dendritic structure formed as a result of independent nucleation events in the undercooled liquid.

It is obvious that the local undercooling is greater in this case and lies outside the coupled growth region, so that nucleation of primary α-Al is favored. It is likely that the coupled growth region is skewed towards higher Cu and Si contents, thus making it somewhat easier to form primary α-Al in hypoeutectic alloys. As one moves away from the wheel-side surface and as the partially solidified ribbon leaves the wheel, the heat extraction rate drops, the solidification rate slows and the dendrites appear coarser. When the heat extraction rate is lower, recalescence from the enthalpy of solidification reduces the undercooling level in the liquid ahead

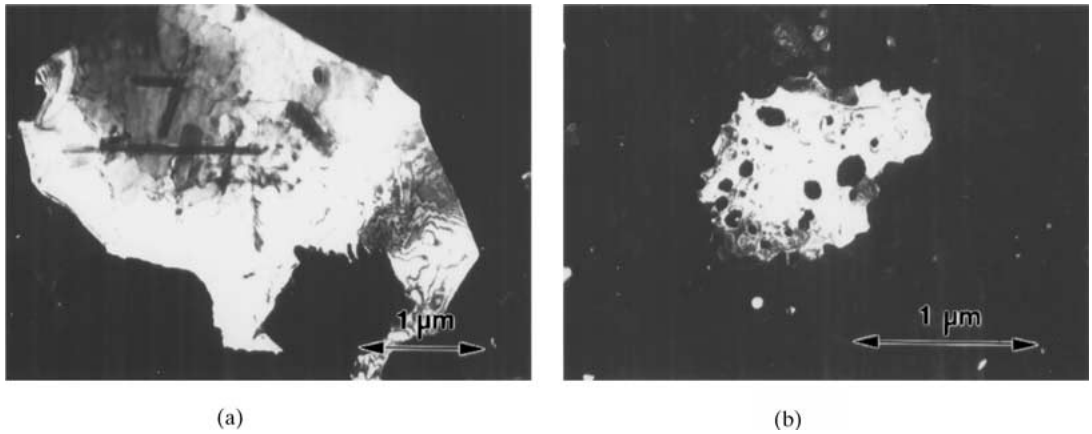

Figure 9 TEM dark field images of Alloy 255 ribbon melt spun at 15 m s^{-1} showing the scale and shape of an α-Al grain. (a) Middle of ribbon. (b) Wheel-side surface.

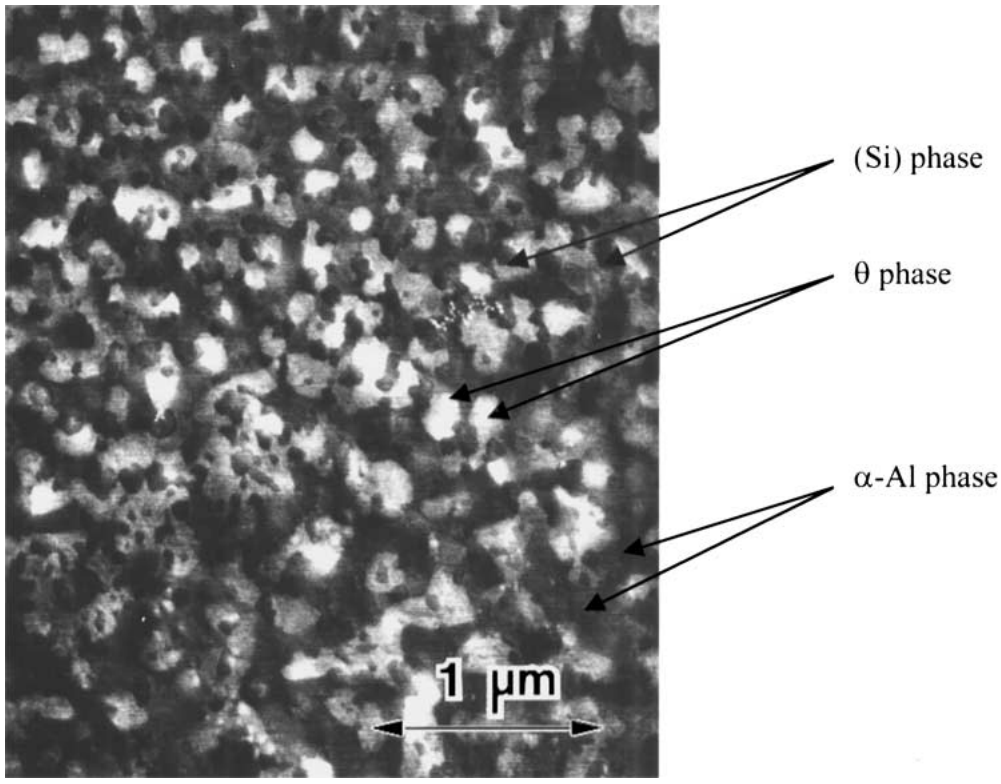

Figure 10 Detail of interlocked eutectic structure in Alloy A255 melt spun ribbon cast at 15 m s^{-1} showing the size, shape and distribution of the three phases.

of the interface. At some critical temperature, the undercooled liquid falls within the coupled growth region of the phase diagram. The liquid then begins to solidify as the interlocked eutectic structure, which appears to involve some sort of cooperative growth. If the solidification rate is rapid enough, the influence of recalescence on interface undercooling is small and the entire ribbon solidifies with a cellular-dendritic structure. It is clear that at the higher cast speed and the associated greater undercooling, the dendritic morphology is preferred. At lower cast speeds and more modest undercoolings, the interlocked eutectic structure is favored.

Studies have shown that the interlocked eutectic structure is very suitable for superplastic deformation. Superplasticity was demonstrated in Pb-62%Sn by Zelin and Mukherjee [12] and in Zn-22%Al by Astanin *et al*. [13]. In both alloys the interlocked eutectic structure was developed via thermomechanical processing. Superplasticity is achieved through sliding and rotation of grain groups and correlated migration of grain boundaries. The dual-phase structure of the interlocked eutectic promotes grain boundary sliding and grain rotation. A dendritic structure does not offer the slip systems necessary for superplasticity.

The scale of the microstructure is also important. Finer grain and phase sizes and eutectic spacings yield enhanced superplastic behavior. Whereas increasing the wheel speed reduced the eutectic spacing, it promotes the undesired dendritic morphology. We varied the copper content of the alloy to determine its influence on the eutectic volume fraction and the eutectic spacing. As expected, the eutectic volume increased to 100% as the copper content approached the ternary eutectic composition. However, the eutectic spacing decreased with increasing copper content, with the smallest spacing forming in the ternary eutectic alloy. The increase in eutectic volume fraction with copper content is predicted by the phase diagram, and it appears in rapidly solidified melt spun ribbons when cast with the intermediate wheel speed. The reduction in eutectic spacing with increasing copper content is not easily explained. This result may be associated with differences in volume fraction of the two phases. Whereas increasing the copper content increases the percentage of eutectic structure and decreased the scale of the microstructure, the volume of the hard θ phase increases which is undesirable as it embrittles the ribbon. Hence, a balance must be achieved between the volume fraction of eutectic and the volume of the θ and (Si) phases to obtain optimum superplastic behavior. With the proper solidification rate and alloy composition, the required microstructural balance of high volume of eutectic and about 30% by volume of the hard (θ + Si) phases in rapidly solidified Al-Cu-Si should be achieved.

Our SEM and TEM results show that the interlocked eutectic structure is made up of a branched θ phase skeleton within an α-Al matrix. The (Si) phase appears within or attached to the intermetallic θ phase but not within the Al-rich phase. The grain size of the Al phase will affect superplasticity. Whereas the largest α-Al grains tend to be larger (approx. 8 μm), the presence of sub-grains is encouraging. If the sub-grain boundaries are relatively high angle, then superplasticity will be enhanced even with these larger grains.

Structures similar to the interlocked eutectic have been observed in rapidly solidified Al-Cu binary eutectic and other eutectic alloy systems and various formation mechanisms have been proposed [11, 14–22]. One common feature of these studies was that the interlocked structure usually formed when

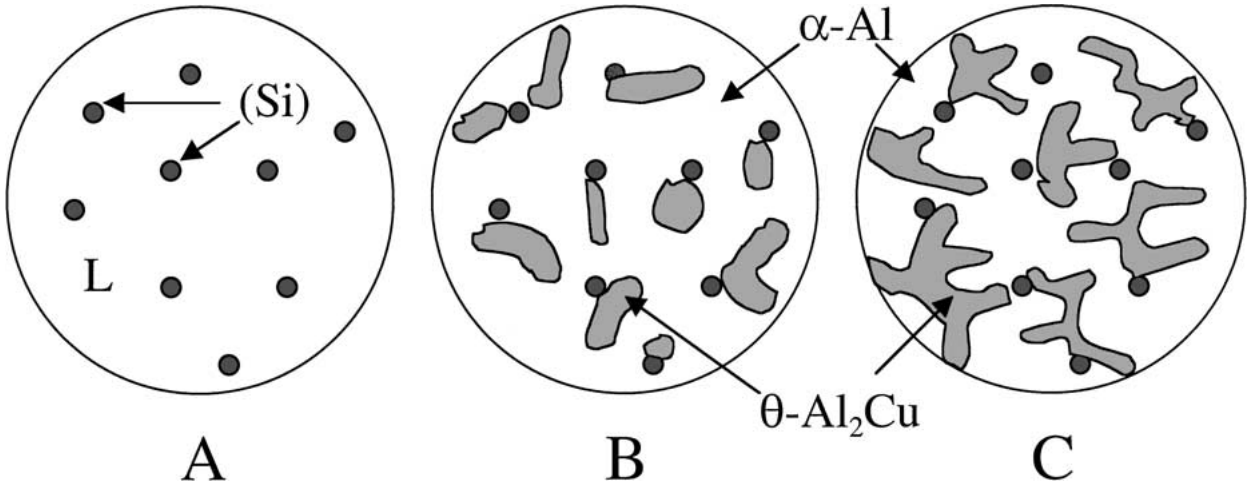

Figure 11 Proposed solidification mechanism in Al-Cu-Si alloys that leads to the interlocked eutectic structure. The (Si) phase forms as a discontinuous phase, whereas the α and θ phases form cooperatively.

solidified at intermediate undercooling level or growth rate which supports our results. Some of the proposed formation mechanisms for the interlocked eutectic structure are solidification of liquid droplets at the grooves of a moving cellular interface, differences in growth rates of the two phases, and fragmentation of primary eutectic lamellae. The last mechanism appears highly unlikely because the growth rates are rapid and the fluid flow required for fragmentation is minimal. Another possible mechanism is precipitation from a rapidly solidified supersaturated Al-rich phase. We discount precipitation as a mechanism because the interlocked structure appears to be primarily interconnected and the θ phase does not appear to exhibit ordered, crystallographically-oriented relationship with the α-Al matrix. The interlocked eutectic structure could not have originated from intercellular liquid drops because the observed structure appears uniformly distributed throughout the microstructure and does not appear to follow any cellular growth direction or cell boundary.

A schematic representation of a proposed mechanism for the formation of the interlocked eutectic structure in Al-Cu-Si ternary alloys is illustrated in Fig. 11. First, the high-melting, (Si) phase forms in the undercooled liquid as a uniformly distributed particulate phase, as shown in diagram A. Near the wheel-side surface, where the cooling and solidification rates are highest, the θ phase is discontinuous and exhibits only a modest degree of branching. This suggests a discontinuous mode of solidification via a multiple nucleation mechanism, as shown in diagram B. In the early stages of the freezing of the ribbon, the growth rate is very high and there is little opportunity for the θ phase to branch significantly. Away from the wheel surface, the growth rate is lower and branching dominates the solidification process. A continuous interlocked structure then results, as shown in diagram C. The branching in the interlocked structure is not like that observed in a dendritic morphology, where the branches are arranged in a tree-like, crystallographically-oriented configuration. The branching we observe is randomly arranged. The interlocked eutectic, which consists of the α-Al + θ phase binary, forms as a result of a combination of two factors: multiple nucleation of the θ phase and a difference in the growth velocities of the α and θ phases. We postulate that the primary (Si) phase particles serve as sites for nucleation of the θ phase, which is suggested by the close association between the θ and (Si) phases in the microstructure. The bct θ phase forms cylindrical-shaped morphologies that appear to undergo a series of random reorientations. Near the wheel side surface, the reorientations are discontinuous, whereas away from the wheel surface they are continuous. The branching may be facilitated by the presence of a third phase, which in this case is (Si), but in binary systems, it could be an impurity phase. In some of the previous studies, impurities have been assumed to be the cause of eutectic structures that are not lamellar.

6. Conclusions

Rapid solidification processing has been employed to generate microstructures that would be useful for the superplastic consolidation of aluminum alloys. Fine-grained, multi-phase interlocked structures have been obtained without thermomechanical processing. By varying the solidification rate (melt spinning wheel speed) and alloy composition (Cu and Si contents) processing conditions have been identified that promote formation of the eutectic structure containing an optimum fraction of the hard phases.

Hypoeutectic compositions and low casting speeds tend to favor the desirable interlocked eutectic structure. Higher casting speeds favored the undesirable dendritic structure, which results from a multiple nucleation process in the deeply undercooled liquid. The preferred interlocked eutectic structure appears to result from multiple nucleation of the θ-Al_2Cu phase and coupled or cooperative growth with the α-Al phase in a modestly undercooled liquid. Sites for the multiple nucleation of the θ phase were provided by a dispersion of (Si) phase spheroids, which are the first crystals to solidify from the undercooled melt. This mechanism for the formation of the interlocked eutectic structure is not firmly established. The present study justifies a more detailed analysis of such a solidification structure. Further work will involve establishment of the orientation and crystallographic relationships between the various

phases and branches, and detailed analysis of the interphase and grain boundaries.

Acknowledgements

The authors wish to thank J. D. Ayers for his guidance and R. Vardiman for performing the transmission electron microscopy.

References

1. J. WADSWORTH, T. G. NIEH and A. K. MUKHERJEE, in "Aluminum Alloys: Their Physical and Mechanical Properties, Vol. 2," edited by E. A. Starke and T. H. Sanders (Chameleon Press, London, 1986) p. 1239.
2. O. D. SHERBY and J. WADSWORTH, in "Deformation, Processing and Structure," edited by G. Krauss (ASM, Materials Park, OH, 1984) p. 355.
3. T. G. NIEH and J. WADSWORTH, *JOM* (1992) 46.
4. J. WADSWORTH and A. R. PELTON, *Scripta Metall.* **18** (1984) 387.
5. S. KAVESH, in "Metallic Glasses," edited by J. J. Gilman and H. J. Leamy (ASM, Metals Park, OH, 1978) p. 37.
6. P. DUWEZ, *ASM Trans.* **60** (1967) 607.
7. M. COHEN and R. MEHRABIAN, in "Rapid Solidification Processing: Principles and Technologies, III," edited by R. Mehrabian (NBS, Gaithersburg, MD, 1982) p. 1.
8. B. E. SUNDQUIST, R. BRUSCATO and L. F. MONDOLFO, *J. Inst. Metals* **91** (1962) 204.
9. M. ZIMMERMANN, M. CARRARD and W. KURZ, *Acta Metall.* **37**(2) (1989) 3305.
10. D. L. HOLT and W. A. BACKOFEN, *ASM Trans.* **59** (1966) 755.
11. L. F. MONDOLFO, "Aluminum Alloys: Structure and Properties" (Butterworths, London, 1976) p. 513.
12. M. G. ZELIN and A. K. MUKHERJEE, *Acta Metall. Mater.* **43**(6) (1995) 2359.
13. V. V. ASTANIN, O. A. KAIBYSHEV and S. N. FAIZOVA, *ibid.* **42**(8) (1994) 2617.
14. I. S. MIROCHNICHENKO, *Russian Metallurgy (Metally)* (5) (1968) 128.
15. W. T. KIM, B. CANTOR and T. H. KIM, *Int. J. Rapid Solid.* **5** (1990) 251.
16. P. TODESCHINI, G. CHAMPIER and F. H. SAMUEL, *J. Mater. Sci.* **27** (1992) 3539.
17. R. GOETZINGER, M. BARTH and D. M. HERLACH, *Acta Metall. Mater.* **46**(5) (1998) 1647.
18. D. SHECHTMAN, W. J. BOETTINGER, T. Z. KATTAMIS and F. S. BIANCANIELLO, *Acta Metall.* **32**(5) (1984) 749.
19. W. J. BOETTINGER, L. A. BENDERSKY, R. J. SCHAEFER and F. S. BIANCANIELLO, *Met. Trans.* **19A** (1988) 1101.
20. W. J. BOETTINGER, *Mats. Sci. & Eng.* **98** (1988) 123.
21. K. P. COOPER, I. E. ANDERSON and J. H. PEREPEZKO, in Proceedings of the Fourth International Conference on Rapidly Quenched Metals (Sendai, Japan, 1981) p. 107.
22. R. CHEESE and B. CANTOR, *Mats. Sci. & Eng.* **45**(1) (1980) 83.

Received 19 April
and accepted 3 August 2001